Charge gradient microscopy

Seungbum Hong[a,b,1], Sheng Tong[b], Woon Ik Park[a,b], Yoshiomi Hiranaga[c], Yasuo Cho[c], and Andreas Roelofs[b,1]

[a]Materials Science Division and [b]Nanoscience and Technology Division, Argonne National Laboratory, Lemont, IL 60439; and [c]Research Institute of Electrical Communication, Tohoku University, Sendai 980-8577, Japan

Edited* by George William Crabtree, Argonne National Laboratory, Chicago, IL, and approved March 28, 2014 (received for review December 30, 2013)

Here we present a simple and fast method to reliably image polarization charges using charge gradient microscopy (CGM). We collected the current from the grounded CGM probe while scanning a periodically poled lithium niobate single crystal and single-crystal $LiTaO_3$ thin film on the Cr electrode. We observed current signals at the domains and domain walls originating from the displacement current and the relocation or removal of surface charges, which enabled us to visualize the ferroelectric domains at a scan frequency above 78 Hz over 10 μm. We envision that CGM can be used in high-speed ferroelectric domain imaging and piezoelectric energy-harvesting devices.

screen charge | atomic force microscopy | piezoresponse | charge scraping

Ferroelectric and piezoelectric materials have attracted great attention due to their applications in commercial markets such as a medical imaging (1–3), next generation inkjet printer heads (4), precision-positioning stages (5, 6), fuel injectors in diesel engines (7, 8), and memory devices (9, 10). The macroscopic properties of ferroelectric and piezoelectric materials that make them appealing for current and future technologies can be more fully understood and improved through detailed knowledge of their domain structures at the nanoscale and mesoscale (11–15).

For example, one well-established microscopy technique that has been applied extensively to ferroelectric materials is Piezoresponse Force Microscopy (PFM), a scanning probe technique that enables the visualization and manipulation of ferroelectric domain structures at the nanoscale (16–18). PFM uses an external ac voltage to modulate the strain induced by the converse piezoelectric effect while monitoring the resulting deformation wave in terms of both amplitude and phase through a lock-in amplifier, which enhances the inherently small vibration signal (19–22). However, one of the major drawbacks of PFM is that the speed of data acquisition is limited by the resonance frequency of the cantilever and the time constant of the lock-in amplifier (23). Very few groups acquired PFM images at scan frequencies higher than 10 Hz over a scan length of 10 μm (24).

To address this challenge, we introduce charge gradient microscopy (CGM), a high-speed nanoscale tool to image ferroelectric and piezoelectric domains. CGM collects the charges that screen either the scraped charges near the tip or the electric polarization beneath the sample surface and maps them as a function of position.

Fig. 1 shows the principle of CGM. Using an atomic force microscopy (AFM), we apply a constant force (F) to the AFM tip and collect current through an amplifier as the tip is scanned across the domain boundaries in a ferroelectric or piezoelectric material. We expect the measured current to have contributions from displacement currents (when crossing over domain boundaries), piezoelectric charge flow, and current due to removal of bound screening charges (25). As CGM does not require a lock-in amplifier as for conventional PFM, it can use higher scan frequencies to obtain domain images. In addition, this technique is different from either conducting AFM (C-AFM) (11) or current-sensing AFM (CS-AFM) (26) in the sense that no external bias is applied while collecting the current and the removal of the surface screening charge by the tip is required (*SI Appendix*, Fig. S1).

CGM images of a periodically poled lithium niobate (PPLN) single crystal are shown in Fig. 2 as a function of scan frequency. It can be clearly seen that the CGM signal is dependent on the scan frequency and that the current increases with the scan speed. We observed two contributions to the CGM signals. The dominant part of the signals at lower scan frequency originates from the displacement current when the tip crosses the domain boundaries (*SI Appendix*, Fig. S2). The second contribution, which becomes stronger as we increase the scan frequency, is believed to originate from the charge flow from the ground to compensate either the overcharged tip (*SI Appendix*, Fig. S3) or the unscreened surface (*SI Appendix*, Fig. S4) when the tip scrapes the surface charges (25). The distortion in the CGM measurements seen in Fig. 2*C* can be explained by the mechanical deformation of platinum tips as observed by scanning electron microscopy (SEM). To ensure that there is no significant capacitance change due to the topography, we measured the rms roughness of the area of interest. The roughnesses were 0.15 and 0.35 nm for PPLN and congruent lithium tantalate (CLT), respectively (*SI Appendix*).

We repeated CGM imaging eight times at a scan frequency of 10 Hz and found that after the first two consecutive scans, there was no significant change in the shape of the current profile. The difference between the first two scans and the rest of the six scans lies in the signal from the domain itself. We noticed that the current on the domain increased and saturated by 0.5 pA in Fig. 2*D*. This is in agreement with the surface potential evolution as a function of number of scans using grounded tip on prewritten domains reported by Kim et al. (27). It should be noted that CGM does not work for the case where the screening mainly takes place through internal screening as supported by the CGM images of

Significance

Polarization charges of ferroelectric materials are screened by an equal amount of surface charges with opposite polarity in ambient condition. Here we show that scraping, collecting, and quantifying the surface screen charges reveals the underlying polarization domain structure at high speed, a technique we call charge gradient microscopy. The scraped charge, measured as a current that scales with scraping rate, induces a charge gradient which leads to the immediate relocation or refill of the screen charges from the vicinity of the probe, making this method a reliable tool to study the complex dynamics of domain nucleation and growth induced by a biased tip in the absence of surface screen charges.

Author contributions: S.H. and A.R. designed research; S.H., S.T., W.I.P., Y.H., Y.C., and A.R. performed research; S.H., S.T., W.I.P., Y.H., Y.C., and A.R. analyzed data; and S.H., S.T., W.I.P., Y.C., and A.R. wrote the paper.

The authors declare no conflict of interest.

*This Direct Submission article had a prearranged editor.

Freely available online through the PNAS open access option.

[1]To whom correspondence may be addressed. E-mail: hong@anl.gov or roelofs@anl.gov.

This article contains supporting information online at www.pnas.org/lookup/suppl/doi:10.1073/pnas.1324178111/-/DCSupplemental.

www.pnas.org/cgi/doi/10.1073/pnas.1324178111

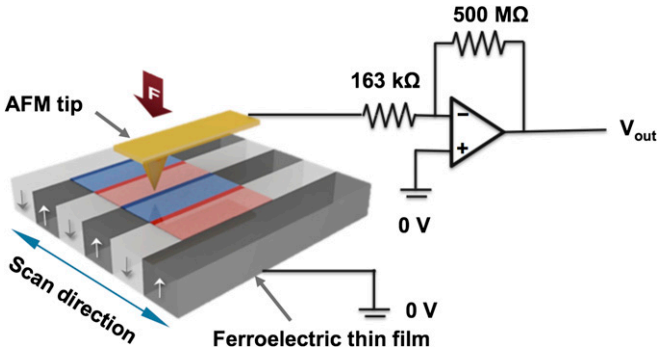

Fig. 1. Schematic diagram of CGM. CGM can characterize polarization charges with a high speed by scraping the screen charges on the surface of the ferroelectric thin film using a conducting AFM tip.

PPLN obtained in vacuum after in situ heat treatment (*SI Appendix*, Figs. S5 and S6).

By integrating the current over the line profile shown in Fig. 2*D* at scan frequency of 10 Hz, we were able to calculate the charge collected to be 45.4 ± 3.3 fC. We calculated the expected displacement charge associated with crossing over a single domain based on the assumption of a hemispherical tip contact with a radius of 45 nm, a remnant polarization (P_r) of 80 μC/cm^2 (28), and an absence of screen charge by surface charge removal (*SI Appendix*, Figs. S1 and S15) (25). The estimated surface charge [$Q = \sigma A = (P_r \bullet n)A$, where σ is surface charge density, A is the area of contact, and n is the unit surface normal vector of A] created by the sample remnant polarization of 80 μC/cm^2 over an area of hemisphere with a radius of 45 nm is 5.05 fC. Because the change of polarization across the domain boundary is $2P_r$, the expected amount of charge flowing to the tip would be 10.1 fC. This leads to the estimated charge of 50.5 fC for five domain walls. The assumption of no screen charge is supported by the fact that we needed to apply at least 1 μN (~120 MPa), which effectively removed the surface screen charge (25) and electrostatic force microscopy (EFM) images we collected before and after the CGM experiments on the PPLN sample (*SI Appendix*, Fig. S1).

We also calculated the expected charge from direct piezoelectric effect, which is 0.007–0.019 fC under the load of 1.17 μN for single-crystal Z-cut lithium niobate with a piezoelectric coefficient, d_{33}, of 6–16 pC/N (29). These calculations [45.4 fC (experiment) vs. 50.5 fC (unscreened displacement charge) and 0.019 fC (piezoelectric charge)] demonstrate that the measured signal is dominated by the unscreened displacement charge across domain walls at a scan frequency of 10 Hz.

We measured the delta current, which is defined to be the difference between the maximum and minimum currents in Fig. 2, as a function of scan frequency from 5 to 30 Hz (*SI Appendix*, Fig. S9). As shown in Fig. 3, we could obtain a linear relationship between the delta current and the scan frequency. As the displacement current linearly scales with the tip velocity, this clearly shows that our method is suitable for high-speed measurement, and we were only limited by the mechanical resonance frequency of our current equipment.

To prove its high-speed capability and the mechanism of collecting displacement current, we used a conducting diamond tip (CDT-NCHR-10, 73 N/m, Nanosensors, Inc.) with the tip load of 41.4 μN and increased the scan frequency to 78.12 Hz over a 10 × 10-μm area on the PPLN sample while collecting both trace (from left to right) and retrace (from right to left) images. The scan angle was fixed at 90° to maximize the charge gradient across the domain boundaries.

As can be seen from Fig. 4 *A* and *B*, the current peaks are located at the domain walls with its positive peak corresponding to the tip moving from positive (upward) domain (dark violet color) to negative (downward) domain (bright yellow color), and its negative peak corresponding to the tip moving from negative to positive domain (*SI Appendix*, Fig. S2).

Finally, we attempted to decrease the feature size of artificially decorated domains in CLT thin films to determine the spatial resolution of CGM. As seen in Fig. 5, features down to about 200 nm are visible, which is comparable to the domain wall width measured in Fig. 4. Compared with the PFM resolution of about 10 nm, this relatively large value implies that the probe should be improved for the nanometer-scale measurement of domains. We envision that we can improve the spatial resolution of CGM down to 20 nm using a tip that separates the function of scraping the screen charge and detecting the current flow. The fundamental limit will be determined either by the bandwidth of the current amplifier (*SI Appendix*, Fig. S10) and contact area of the tip (*SI Appendix*, Fig. S11) and the sample surface or by the domain wall thickness. The optimization of the process

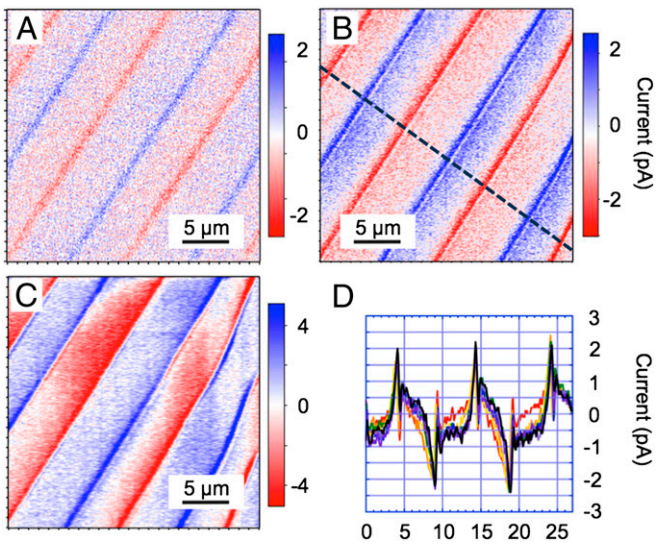

Fig. 2. CGM images as a function of scan frequency: (*A*) 5 Hz, (*B*) 10 Hz, and (*C*) 20 Hz over an area of 25 × 25 μm on the PPLN single crystal. (*D*) Repeatability of CGM imaging. Line profiles obtained on the same region across the black dotted line in *B* with number of repetitions: 1, red; 2, orange; 3, yellow; 4, green; 5, blue; 6, indigo; 7, violet; and 8, black. The width of each domain is 5 μm.

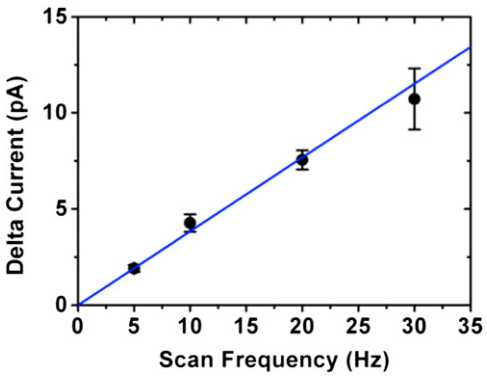

Fig. 3. Delta current as a function of scan frequency. The difference between maximum and minimum current values, i.e., delta current in the line profiles, is plotted as a function of scan frequency from 5 to 30 Hz. Ten delta current values were averaged in each data point.

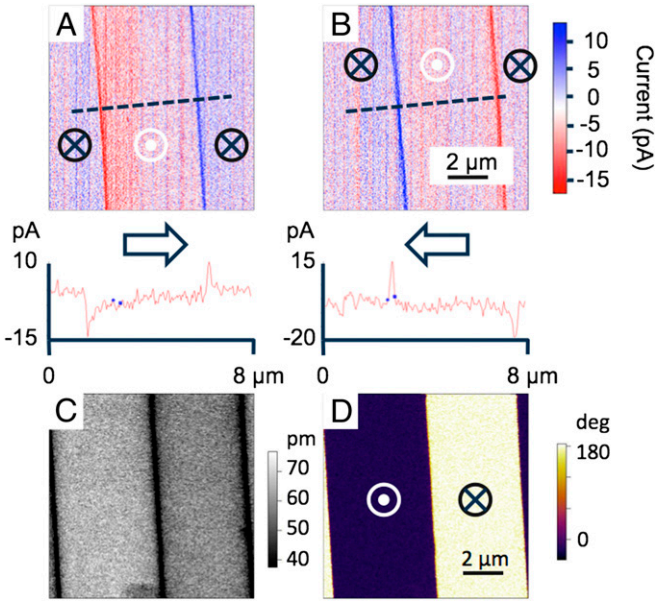

Fig. 4. Trace and retrace CGM images at scan frequency of 78 Hz. CGM images taken on domain boundaries of PPLN sample from (*A*) left-to-right scan (trace) and (*B*) right-to-left scan (retrace) with line profiles showing the current peaks at domain boundaries. PFM (*C*) amplitude and (*D*) phase images are taken at the same region where dark phase contrast corresponds to positive (upward) domain and bright phase contrast corresponds to negative (downward) domain.

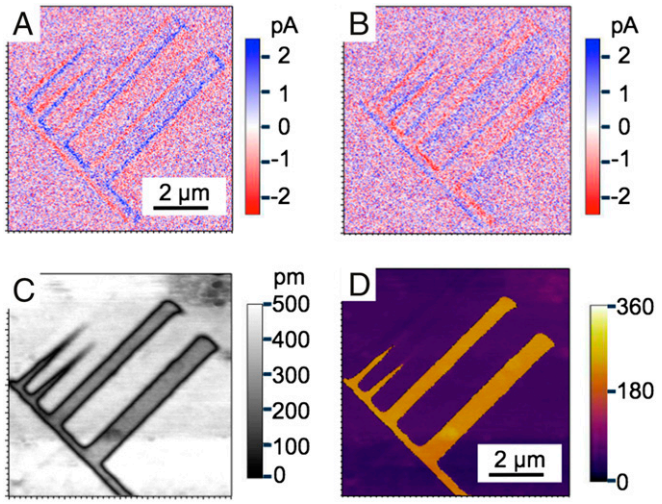

Fig. 5. Trace and retrace CGM images of artificially decorated domains with different sizes. CGM images taken on ribbon-shaped domains poled by 6 V to the bottom electrode of 85-nm-thick $LiTaO_3$ films from (*A*) left-to-right scan (trace) and (*B*) right-to-left scan (retrace) using Pt tips at scan frequency of 40 Hz. PFM (*C*) amplitude and (*D*) phase images are taken at the same region at scan frequency of 1 Hz where bright phase contrast corresponds to positive (upward) domain and dark phase contrast corresponds to negative (downward) domain. A real-time acquisition movie of CGM images is available (Movie S1).

parameters and tip geometry is underway to improve the spatial resolution.

We did not observe any significant milling effect by mechanical indentation on the PPLN sample when using the Pt tip. However, we observed such an effect when using a conducting diamond-coated tip with a load over 40 μN. From this observation combined with the EFM images obtained before and after the CGM experiments (*SI Appendix*, Fig. S1), we believe that the screening charges can be scraped mechanically by the AFM tip.

In conclusion, CGM is a simple and fast scanning probe microscopy that can characterize polarization domains by scraping the screen charges on the surface using a conducting nanoscale tip. As such, CGM opens possibilities for investigating unscreened surfaces without the need of using ultrahigh vacuum systems. Furthermore, we envision that a CGM-based energy harvester can be designed.

Materials and Methods

Calibration of Conducting AFM. Before conducting CGM, first we carried out calibration of our C-AFM to check the nature of contact (Ohmic or Schottky), contact resistance, and offset in both voltage and current measurement using highly ordered pyrolytic graphite (HOPG) standard sample (ZYB, NT-MDT) (*SI Appendix*, Fig. S12).

CGM Experiments on PPLN Single-Crystal Sample. After the calibration, we performed our CGM imaging using grounded Pt-wire tips (RMN 25Pt300B, 18 N/m, Rocky Mountain Nanotechnology, LLC) on a periodically poled lithium niobate sample (PPLN, AR-PPLN test sample, Asylum Research, Inc., which consists of a 3 × 3-mm $LiNbO_3$ transparent die that is 0.5 mm thick). The current was collected through the AFM tip attached to the cantilever holder (ORCA, gain of 5×10^8 volts/amp (~1 pA to 20 nA), Asylum Research) while the bottom electrode was grounded. To make sure the tip was grounded, we removed the offset voltage of about −83 mV presented in the system. We also removed the offset current of about 50 pA.

The scan frequency was varied from 5 to 30 Hz, and the scan size was 25 × 25 μm. The applied force to the tip was 1.17 μN. The scan angle was fixed at 45°. The CGM image consisted of 256 × 256 pixels. To obtain line profiles across the domain boundaries, an arbitrary line perpendicular to the domain wall was chosen. To get better signal-to-noise ratio, 20 lines adjacent to the arbitrarily chosen line were used to get the averaged line profile.

CGM Experiments on CLT Thin Films. To see if we can apply the CGM to other ferroelectric materials, we have obtained very thin and uniform CLT thin films with thicknesses of 30–100 nm on 500-nm-thick Cr electrodes, of which preparation details can be found in the *SI Appendix*. For CGM images on CLT thin films, we used Pt-wire tips. The scan frequency was 39.06 Hz, and the scan size was 8 × 8 μm. The scan angle was fixed at 45°. The load applied to the tip was 1.17 μN. Both trace (from left to right) and retrace (from right to left) scans were imaged. CGM images of artificially decorated squares and circles with different sizes at a scan frequency of 156 Hz were also obtained (*SI Appendix*, Fig. S13).

PFM Imaging of PPLN Single-Crystal and CLT Thin Film Samples. As a control experiment, we performed conventional out-of-plane PFM on the PPLN sample using drive frequency of 426.54 kHz and drive voltage of 1 V to the Pt-wire tip (*SI Appendix*, Fig. S14). For CLT thin films, we obtained PFM images (Fig. 5) using conducting diamond-coated silicon cantilever (CDT-NCHR-10, Nanosensors, Inc.) with ac bias voltage of 2 V and 70 kHz to the bottom electrode, scan frequency of 2 Hz, and applied force of 2.3 μN.

ACKNOWLEDGMENTS. The authors acknowledge stimulating discussions with S. Hruszkewycz at Argonne National Laboratory, S. H. Baek at Korea Institute of Science and Technology, Korea, and B. Rodriguez at Trinity College, Ireland. The work was supported by the US Department of Energy, Office of Science, Materials Sciences and Engineering Division and by the Center for Nanoscale Materials, a US Department of Energy, Office of Science, Office of Basic Energy Sciences User Facilities under Contract DE-AC02-06CH11357. The CGM and PFM in the main text and CGM/PFM/EFM/C-AFM in ambient condition in the *SI Appendix* were performed at Materials Science Division and the vacuum PFM and CGM and SEM (S.H., S.T., and W.I.P.) in the *SI Appendix* were performed at the Center for Nanoscale Materials and Electron Microscopy Center. We acknowledge Y.-Y. Choi and J. R. Guest at Argonne National Laboratory for their support in CGM experiments.

1. Szabo TL (2004) *Diagnostic Ultrasound Imaging: Inside Out* (Academic Press, Burlington, VT).

2. Huang D, et al. (1991) Optical coherence tomography. *Science* 254(5035):1178–1181.

3. Fujimoto JG (2003) Optical coherence tomography for ultrahigh resolution in vivo imaging. *Nat Biotechnol* 21(11):1361–1367.
4. Wijshoff H (2010) The dynamics of the piezo inkjet printhead operation. *Phys Rep* 491:77–177.
5. Purcell TJ, Sweeney HL, Spudich JA (2005) A force-dependent state controls the coordination of processive myosin V. *Proc Natl Acad Sci USA* 102(39):13873–13878.
6. Pauzauskie PJ, et al. (2006) Optical trapping and integration of semiconductor nanowire assemblies in water. *Nat Mater* 5(2):97–101.
7. Cross E (2004) Materials science: Lead-free at last. *Nature* 432(7013):24–25.
8. Payri R, Gimeno J, Viera JP, Plazas AH (2013) Needle lift profile influence on the vapor phase penetration for a prototype diesel direct acting piezoelectric injector. *Fuel* 113:257–265.
9. Kim YS, et al. (2013) Advanced wafer thinning technology and feasibility test for 3D integration. *Microelectron Eng* 107:65–71.
10. Ng TN, et al. (2012) Scalable printed electronics: An organic decoder addressing ferroelectric non-volatile memory. *Sci Rep* 2:585.
11. Seidel J, et al. (2010) Domain wall conductivity in La-doped $BiFeO_3$. *Phys Rev Lett* 105(19):197603.
12. Zeches RJ, et al. (2009) A strain-driven morphotropic phase boundary in $BiFeO_3$. *Science* 326(5955):977–980.
13. Jang HW, et al. (2010) Ferroelectricity in strain-free $SrTiO_3$ thin films. *Phys Rev Lett* 104(19):197601.
14. Kalinin SV, Morozovska AN, Chen LQ, Rodriguez BJ (2010) Local polarization dynamics in ferroelectric materials. *Rep Prog Phys* 73:056502.
15. McQuaid RGP, McGilly LJ, Sharma P, Gruverman A, Gregg JM (2011) Mesoscale flux-closure domain formation in single-crystal $BaTiO_3$. *Nat Commun* 2:404.
16. Park M, No K, Hong S (2013) Visualization and manipulation of meta-stable polarization variants in multiferroic materials. *AIP Adv* 3:042114.
17. Balke N, et al. (2009) Deterministic control of ferroelastic switching in multiferroic materials. *Nat Nanotechnol* 4(12):868–875.
18. Ievlev AV, et al. (2014) Intermittency, quasiperiodicity and chaos in probe-induced ferroelectric domain switching. *Nat Phys* 10:59–66.
19. Roelofs A, et al. (2000) Differentiating 180° and 90° switching of ferroelectric domains with three dimensional piezoresponse force microscopy. *Appl Phys Lett* 77: 3444–3446.
20. Hong S, et al. (2001) Principle of ferroelectric domain imaging using atomic force microscope. *J Appl Phys* 89:1377–1386.
21. Soergel E (2011) Piezoresponse force microscopy (PFM). *J Phys D Appl Phys* 44:464003.
22. Hruszkewycz SO, et al. (2013) Imaging local polarization in ferroelectric thin films by coherent x-ray Bragg projection ptychography. *Phys Rev Lett* 110(17):177601.
23. Ko H, et al. (2011) High-resolution field effect sensing of ferroelectric charges. *Nano Lett* 11(4):1428–1433.
24. Nath R, et al. (2008) High speed piezoresponse force microscopy: <1 frame per second nanoscale imaging. *Appl Phys Lett* 93:072905.
25. Kim Y, et al. (2008) Screen charge transfer by grounded tip on ferroelectric surfaces. *Phys Stat Sol RRL* 2:74–76.
26. Cho SH, Park SM (2006) Electrochemistry of conductive polymers 39. Contacts between conducting polymers and noble metal nanoparticles studied by current-sensing atomic force microscopy. *J Phys Chem B* 110(51):25656–25664.
27. Kim Y, et al. (2009) Origin of surface potential change during ferroelectric switching in epitaxial $PbTiO_3$ thin films studied by scanning force microscopy. *Appl Phys Lett* 94: 032907.
28. Gopalan V, Mitchell TE, Furukawa Y, Kitamura K (1998) The role of nonstoichiometry in 180° domain switching of $LiNbO_3$ crystals. *Appl Phys Lett* 72:1981–1983.
29. Smith RT, Welsh FS (1971) Temperature dependence of the elastic, piezoelectric, and dielectric constants of lithium tantalate and lithium niobate. *J Appl Phys* 42: 2219–2230.